




# Spatial Correlation Between Myocyte's Repolarization Times and Their Alternans Drives T-Wave Alternans on the ECG

Massimo W. Rivolta , Member, IEEE, Juan Pablo Martínez , Member, IEEE, Roberto Sassi , Senior Member, IEEE, and Pablo Laguna , Fellow, IEEE

## I. INTRODUCTION

**Abstract**—Objective: T-wave alternans (TWA) manifests as beat-to-beat fluctuations of T-wave morphology on the electrocardiogram (ECG), with physiological bases not fully understood. Using a biophysical model of the ECG, we demonstrate and give explicit relations that TWA depends on the i) spatial covariance between myocytes' repolarization time and alternans; and ii) global alternans (common to every myocyte). Methods: We quantified the spatial covariance and global alternans by means of two new metrics,  $\mathcal{R}$  index and  $\bar{\delta}$ , respectively. They were validated on both synthetic and real signals. Computerized simulations were generated using a biophysical model linking the action potentials with the surface ECG. Then, the metrics were computed in STAFF-III dataset, containing ECGs from patients who underwent coronary angioplasty with prolonged balloon inflations, and the time courses of the metrics were analyzed together with TWA measured on the surface ECG. Results: The metrics properly estimated the spatial covariance and global alternans in the synthetic data. In the STAFF-III dataset, the  $\mathcal{R}$  index progressively increased from baseline to the fourth minute of inflation (median  $\Delta\mathcal{R} = 0.81$  ms;  $p < 0.05$ ), whereas  $\bar{\delta}$  was mostly unaltered during the intervention ( $\bar{\delta} = 0$  ms). Conclusion: We reported, for the first time, that TWA is significantly driven by the myocyte's spatial covariance between their repolarization times and alternans, and not by global alternans, when TWA is generated by regional ischemia. Significance: The metrics may reveal new complementary insights into the mechanisms underlying TWA.

**Index Terms**—Action potential duration alternans, ECG, STAFF-III, T-wave alternans, ventricular repolarization.

Manuscript received 6 February 2022; revised 15 June 2022; accepted 21 July 2022. Date of publication 29 July 2022; date of current version 7 November 2022. The work of Juan Pablo Martínez and Pablo Laguna was supported in part by the Spanish Ministry of Science and Innovation (MICINN) and FEDER under Projects PID2019-104881RB-I00 and PID2019-105674RB-I00, and in part by the Gobierno de Aragón (Reference Group BSiCoS T39-20R) through FEDER 2014-2020 Building Europe from Aragón. (Corresponding author: Massimo W. Rivolta.)

Massimo W. Rivolta and Roberto Sassi are with the Dipartimento di Informatica, Università degli Studi di Milano, 20133 Milan, Italy (e-mail: massimo.rivolta@unimi.it; roberto.sassi@unimi.it).

Juan Pablo Martínez and Pablo Laguna are with the BSiCoS Group, Aragón Institute of Engineering Research, IIS Aragón, Universidad de Zaragoza, 50009 Zaragoza, Spain, and also with the CIBER en Bioingeniería, Biomateriales y Nanomedicina (CIBER-BBN), 50018 Zaragoza, Spain (e-mail: jpmart@unizar.es; laguna@unizar.es).

Digital Object Identifier 10.1109/JBHI.2022.3195060

T-WAVE alternans (TWA) manifests as periodic fluctuations of T-wave amplitude and morphology on the surface ECG, occurring on a beat-to-beat basis [1]. It has been associated with sudden cardiac death (SCD) in numerous studies involving different clinical conditions, such as myocardial infarction and ischemia, chronic heart failure, long QT syndrome [2], [3], [4]. However, despite these findings, it is still not clear whether TWA assessment should be used in the clinical setting and a lack of clinical consensus on its use is present as well [5]. The main reason is that the physiological basis generating TWA and its link with SCD are not yet fully understood, especially considering the vast amount of conditions that may be involved, such as genetic mutation, scars due to myocardial infarction, autonomic regulation.

At the cellular level, spatio-temporal alternations in the heterogeneity of ventricular repolarization are mostly due to intracellular calcium handling oscillations [6], [7]. Such oscillations change the shape and duration of the action potentials (APs) and occur at high heart rate (HR) over a certain threshold, being such threshold lower in subjects susceptible to SCD [1]. Malignant arrhythmias may develop in presence of ventricular regions alternating with opposite phase (discordant alternans), which facilitates the onset of electrical reentries [8].

Over the years, numerous indexes and algorithms have been proposed to quantify TWA from the surface ECG, such as Spectral Method, Complex Demodulation Method, Modified Moving Average Method and Laplacian Likelihood Ratio Method. The reader may refer to [9] for a comprehensive review on TWA analysis methods. Besides these ones, for example, Monasterio et al. [3] proposed a multi-lead approach combining a technique called Periodic Component Analysis with the Laplacian likelihood ratio method [2], and obtained a high prognostic power for SCD in a chronic heart failure cohort.

Inferring causation or correlation of ECG-based TWA measurements with physiological quantities is challenging without proper experiments, such as those on *in-vitro* tissue preparations. A possible alternative is the use of mathematical models. In this context, algorithms are meant to solve the inverse problem between the surface ECG and the (typically) thousands of parameters of the models (e.g., [10]). However, such algorithms present several issues related to the intrinsic ill-posedness definition

of the problem that might not provide a physiologically-sound solution.

In the initial part of this work, we demonstrate for the first time, using an electrophysiological model of the surface ECG, that the observed TWA's amplitude depends not only on the repolarization alternans but also on its spatial correlation with the repolarization times. Furthermore, the model hints that a significant role is played by global alternans (*i.e.*, concordant alternans common in magnitude to all myocytes). In the second part, we proposed two metrics to quantify: i) the spatial covariance between repolarization times and repolarization alternans,  $\mathcal{R}$  index, and ii) the global alternans,  $\bar{\delta}$ , in both cases using surface 12-lead ECG. The metrics have been extensively tested with computerized simulations and assessed on real data as well.

## II. METHODS

### A. Background on the Equivalent Surface Source Model

A major advance in understanding how the T-wave on the surface ECG changes its morphology, in relation to alterations in the APs or their repolarization time, is due to the introduction of the equivalent surface source (ESS) model proposed by van Oosterom [11]. According to this model, at beat  $k$ , the T-wave in the surface ECG is represented as a linear combination of the transmembrane APs of the myocytes:

$$\psi_k(t) = \mathbf{A} \begin{bmatrix} d(t - \rho_{k,1}) \\ \dots \\ d(t - \rho_{k,M}) \end{bmatrix}, \quad (1)$$

where  $\psi_k(t) = [\psi_{k,1}(t) \dots \psi_{k,L}(t)]^\top$  is a vector containing the multi-lead surface ECG with  $L$  leads at time  $t$  of the beat  $k$ ,  $M$  is the total number of cells (or nodes) considered in the modeling,  $d(t)$  is the transmembrane potential, assumed identical for each myocyte (assumption that holds during phase 3 of the cardiac action potential, *i.e.*, repolarization),  $\rho_{k,m}$  is the time instant in which the  $m$ -th myocyte can be considered repolarized (conventionally measured from the beginning of the  $k$ -th QRS complex), and  $\mathbf{A}$  is the subject-specific  $L \times M$  constant transfer matrix (sum of each row of  $\mathbf{A}$  is 0; please, refer to [11] for additional mathematical properties).

The model in (1) can be further approximated by decomposing  $\psi_k(t)$  using a Taylor expansion of  $d(t)$  for  $\rho_{k,m}$  around the average repolarization time  $\bar{\rho}_k = \frac{1}{M} \sum_{m=1}^M \rho_{k,m}$ , obtaining

$$\psi_k(t) \approx \mathbf{w}_{1,k} t_{d,k}(t) + \mathbf{w}_{2,k} \dot{t}_{d,k}(t), \quad (2)$$

where  $-t_{d,k}(t)$  is the dominant T-wave (DTW) [12], [13], which results from the time derivative of the transmembrane potential,  $\dot{t}_{d,k}(t) = \dot{d}(t - \bar{\rho}_k)$ , and then

$$\begin{aligned} \mathbf{w}_{1,k} &= -\mathbf{A} \Delta \rho_k \\ \mathbf{w}_{2,k} &= \frac{1}{2} \mathbf{A} (\Delta \rho_k \circ \Delta \rho_k) \end{aligned} \quad (3)$$

are called lead factors ( $L \times 1$  vectors), with  $\Delta \rho_k = [\Delta \rho_{k,1} \dots \Delta \rho_{k,M}]^\top$  a vector containing all  $\Delta \rho_{k,m} = \rho_{k,m} - \bar{\rho}_k$ , *i.e.*, temporal delay of the  $m$ -th myocyte

from the average repolarization time, and with  $\circ$  being the Hadamard (pointwise) product.

From a signal processing perspective, it is worth noting that the approximated model in (2) can be fitted on the T-wave. Indeed, from the  $L \times N$  samples composing the multi-channel ECG, where  $N$  is the number of samples in a given lead, an estimate of  $N + 2L$  model parameters becomes feasible without the need of computing the  $\mathbf{A}$  matrix. Solving the inverse problem in (1) would instead require estimating  $L \times M$  parameters for the matrix  $\mathbf{A}$  and  $M \times N$  parameters for the APs.

### B. Background on $\mathcal{V}$ -Index

Supported by electrophysiological observations obtained from animal cardiac tissue preparations [14], [15], Sassi and Mainardi [16] proposed a statistical model of the repolarization time delay  $\Delta \rho_{k,m}$  consisting of two terms:

$$\Delta \rho_{k,m} = \theta_m + \phi_{k,m}, \quad (4)$$

where  $\theta_m$  represents the constant-in-time repolarization time delay of the  $m$ -th myocyte varying across the myocardial volume, while  $\phi_{k,m}$  is a zero-mean i.i.d. Gaussian random variation  $\sim \mathcal{N}(0, \sigma_\phi^2)$ , that occurs at  $k$ -th beat. While theoretical, the stochastic model is coherent with the fact that, given  $B$  beats, the repolarization time  $\rho_{k,m}$  can always be decomposed as:

$$\rho_{k,m} = \overbrace{\bar{\rho} + \bar{\phi}_k}^{\bar{\rho}_k} + \theta_m + \phi_{k,m}, \quad (5)$$

where  $\bar{\rho} = \sum_{k=1}^B \bar{\rho}_k / B$  is the global average repolarization time, while  $\bar{\phi}_k = \bar{\rho}_k - \bar{\rho}$  captures the deviation of the average repolarization time of the  $k$ -th beat with respect to the global one, with  $\sum_{k=1}^B \bar{\phi}_k = 0$ . Finally,  $\theta_m = \sum_{k=1}^B \rho_{k,m} / B - \bar{\rho}$  and  $\phi_{k,m} = \rho_{k,m} - \bar{\rho} - \bar{\phi}_k - \theta_m$  with  $\sum_k \phi_{k,m} = \sum_m \phi_{k,m} = 0$  by construction.

Using the model in (4), it is possible to show that the spatial variance (*i.e.*, across  $m$ ) of  $\theta_m$  is approximately the ratio of the ensemble variances of the lead factors (which, when stationarity and ergodicity hold, corresponds to the sample variances computed over beats). The latter ratio was termed “ $\mathcal{V}$ -index” [16] and its mathematical formulation, obtained along the lines of what is described in Appendix [17] (but performing the Taylor's expansion in  $\bar{\rho}_k$ , for the special case  $a_m = 0$ ), is as follows

$$v_l^2 = \frac{\text{var}[w_{2,k,l}]}{\text{var}[w_{1,k,l}]} = \frac{\sigma_\phi^2}{2} + s_{\theta\theta} + \eta_{\theta\theta,l}, \quad (6)$$

where  $l$  is the ECG lead,  $s_{xy} = \sum_{m=1}^M (x_m - \bar{x})(y_m - \bar{y}) / M$  is the spatial sample covariance of  $x$  and  $y$ ,  $\sigma_\phi^2$  is the variance of  $\phi_{k,m}$  (usually  $\ll s_{\theta\theta}$ ). The term

$$\begin{aligned} \eta_{xy,l} &= \frac{s_{A_l^2 xy}}{s_{A_l A_l}} \\ &= \frac{\sum_{m=1}^M \left( A_{l,m}^2 - \frac{\sum_{j=1}^M A_{l,j}^2}{M} \right) \left( x_m y_m - \frac{\sum_{j=1}^M x_j y_j}{M} \right)}{\sum_{m=1}^M A_{l,m}^2} \end{aligned} \quad (7)$$

is the ratio between the spatial covariance of  $A_l^2$  with the product  $xy$ , and the spatial covariance of  $A_l$ , which is also much lower than  $s_{\theta\theta}$  given the non-coherent nature of the two quantities  $A_l^2$  and  $xy$  [13]. In practice, the  $\mathcal{V}$ -index is computed as follows

$$\hat{\mathcal{V}} = \frac{1}{L} \sum_{l=1}^L \sqrt{\hat{v}_l^2}, \quad (8)$$

where  $\hat{v}_l^2$  is calculated as the ratio of variances in (6), but using the sample variances (determined on a set of beats) of  $w_{1,k}$  and  $w_{2,k}$ .

### C. A Model of Repolarization Alternans

According to Pastore et al.'s studies on guinea pig hearts, TWA occurs in two different forms depending on the stimulation rate [8], [18]. At lower stimulation rates, repolarization times either prolong or shorten at all sites on a beat-to-beat basis (concordant alternans<sup>1</sup>). If the stimulation rate grows over a critical threshold, repolarization times become less "regular" and those of adjacent myocardial regions may alternate with opposite phase (discordant alternans).

These two phenomena can be modeled extending the ideas of Section II-B, by considering that each myocyte might have a repolarization time oscillating on a beat-to-beat basis. This oscillation thus implies that

$$\mathbb{E} [\rho_{2i,m} - \rho_{2i-1,m}] = a_m = \bar{\delta} + \delta_m, \quad (9)$$

where  $i = \lceil k/2 \rceil$  is the pair index of consecutive beats. The expected value of the difference in the repolarization time of a given myocyte  $m$  in two consecutive beats is the constant-in-time oscillation  $a_m$ , further decomposed in  $\bar{\delta}$ , a global alternans common to every myocyte, and  $\delta_m$ , the alternans component specific to each single cell. Depending on the values of  $a_m$ , it is possible to have both concordant and discordant alternans, as well as isolated regions with alternans. It is worth noting that  $a_m$  is potentially HR dependent [8]. We restrict our considerations to ECG segments at stable HR, thus avoiding to explicitly model such dependency in (9).

The repolarization time model develops by making explicit the alternating term in (5), as follows:

$$\rho_{k,m} = \overbrace{\bar{\rho}_k + \bar{\phi}_k}^{\bar{\rho}_k} + \frac{(-1)^k}{2} \underbrace{(\bar{\delta} + \delta_m)}_{a_m} + \theta_m + \phi_{k,m}. \quad (10)$$

Now, we model  $\bar{\phi}_k$  as a Gaussian variable with mean 0 and variance  $\sigma_{\bar{\phi}}^2$ , i.e.,  $\bar{\phi}_k \sim \mathcal{N}(0, \sigma_{\bar{\phi}}^2)$ ,  $\forall k$ . This model is based on the fact that, under stable HR,  $\bar{\phi}_k$  represents a beat-to-beat variation of the average repolarization time  $\bar{\rho}_k$ , common to all myocytes in the given beat  $k$ , from the global repolarization time  $\bar{\rho}$ . According to the ESS model in (1), shifting all repolarization times of a fixed quantity in a given beat produces a temporal shift in the T-wave, thus leading to a change in the QT interval of that beat. This observation hints that  $\bar{\phi}_k$  captures part of the

<sup>1</sup>Concordant alternans defines prolongations or shortenings as possibly different across sites, but all either positive or negative.

beat-to-beat QT variability. Considering that QT variability has a standard deviation usually lower than 5 ms [19] in healthy subjects at rest, this gives us that  $\sigma_{\bar{\phi}} < 5$  ms.

### D. Expected Value of TWA on the Surface ECG

Under quasi-static conditions, when the matrix  $\mathbf{A}$  is independent from time (no changes in the volume conductor geometry, conductivity and lead positions) and the transmembrane AP  $d(t)$  during repolarization is identical across cells and beats (assuming a stationary HR), TWA observed on the surface ECG is only due to periodic beat-to-beat variations in the spatial distribution of the repolarization times across the myocardial volume.

These assumptions motivate the approximation of the surface ECG using the same mathematical considerations reported in Section II-A. In fact, the contribution of repolarization alternans on the surface ECG can be highlighted by means of a second-order Taylor expansion of  $d(t)$  in  $\bar{\rho}$ , as follows:

$$\begin{aligned} d(t - \rho_{k,m}) &\approx d(t - \bar{\rho}) \\ &- \dot{d}(t - \bar{\rho}) \left[ \theta_m + \bar{\phi}_k + (-1)^k \frac{a_m}{2} + \phi_{k,m} \right] \\ &+ \frac{1}{2} \ddot{d}(t - \bar{\rho}) \left[ \theta_m + \bar{\phi}_k + (-1)^k \frac{a_m}{2} + \phi_{k,m} \right]^2. \end{aligned} \quad (11)$$

Here, it is worth noting that, differently from the  $\mathcal{V}$ -index formulation, the approximation depends on a single DTW  $-t_d(t) = -\dot{d}(t - \bar{\rho})$  common to all beats.

Consequently, the surface ECG can be approximated as follows:

$$\begin{aligned} \psi_k(t) &\approx w_{1,k} t_d(t) + w_{2,k} \dot{t}_d(t) \\ w_{1,k} &= -\mathbf{A} \left[ \boldsymbol{\theta} + \bar{\phi}_k \mathbf{1} + (-1)^k \frac{\mathbf{a}}{2} + \boldsymbol{\phi}_k \right] \\ w_{2,k} &= \frac{1}{2} \mathbf{A} \left[ \left( \boldsymbol{\theta} + \bar{\phi}_k \mathbf{1} + (-1)^k \frac{\mathbf{a}}{2} + \boldsymbol{\phi}_k \right) \right. \\ &\quad \left. \circ \left( \boldsymbol{\theta} + \bar{\phi}_k \mathbf{1} + (-1)^k \frac{\mathbf{a}}{2} + \boldsymbol{\phi}_k \right) \right] \end{aligned} \quad (12)$$

where  $w_{1,k}$  and  $w_{2,k}$  are the lead factors, and  $\boldsymbol{\theta}$ ,  $\boldsymbol{\phi}_k$ , and  $\mathbf{a}$  are  $M$  dimensional vectors containing all the  $\theta_m$ ,  $\phi_{k,m}$  and  $a_m$  values, respectively.

By taking the expected value of the difference between the approximated surface ECG of even and odd beats, it is possible to show that the expected value of TWA is

$$\begin{aligned} &\left| \mathbb{E} [\psi_{2i,l}(t) - \psi_{2i-1,l}(t)] \right| \\ &\approx \left| -t_d(t) \sum_{m=1}^M A_{l,m} \delta_m + \dot{t}_d(t) \sum_{m=1}^M A_{l,m} \theta_m (\bar{\delta} + \delta_m) \right|, \end{aligned} \quad (13)$$

where  $\psi_{k,l}(t)$  is the  $l$ -th lead of the surface ECG at time  $t$  and  $k$ -th beat. TWA depends on the spatial variation of repolarization alternans  $\delta_m$ , and the product of the alternans  $a_m$  with the spatial distribution of repolarization delay  $\theta_m$ , in both cases weighted by the matrix  $\mathbf{A}$ .

### E. Alternating $\mathcal{V}$ -Index and the $\mathcal{R}$ Index

In an animal model comprising of guinea pigs, Choi and Salama [6] observed a correlation coefficient of around 0.7 between repolarization alternans and the action potential duration. This result implies the existence of a spatial covariance (across myocytes) between these two quantities and, reasonably, a spatial covariance between repolarization alternans and repolarization times  $s_{\theta\delta}$  might exist too. Such spatial covariance  $s_{\theta\delta}$  could be a meaningful measure for the stratification of patients at risk of SCD, that is clearly visible after expressing  $s_{\theta\delta}$  as function of  $s_{\theta\theta}$ ,  $s_{\delta\delta}$  and the Pearson's correlation coefficient  $p_{\theta\delta}$ ,  $s_{\theta\delta} = p_{\theta\delta} \sqrt{s_{\theta\theta} s_{\delta\delta}}$ . Indeed,  $s_{\theta\theta}$  quantifies the spatial heterogeneity of ventricular repolarization (it is what the  $\mathcal{V}$ -index estimates) and it is known to be associated with higher risks of SCD. High values of  $s_{\delta\delta}$  are also expected to increase the risk given the fact that a higher variance of repolarization alternans would lead to higher TWA (see the expected value of TWA in (13)). Finally, the parameter  $p_{\theta\delta}$  modulates the spatial covariance between  $\theta$  and  $\delta$ .

The lead factors reported in (12) can be used to obtain the  $\mathcal{V}$ -index for even and odd beats, *i.e.*,  $v_{2i,l}^2$  and  $v_{2i-1,l}^2$  for each lead  $l$ . In general, these two quantities would be equivalent, but with alternans, we expect a difference in the  $\mathcal{V}$ -index computed on even and odd beats. In fact, the difference, as reported in Appendix [17], is

$$|v_{2i,l}^2 - v_{2i-1,l}^2| = 2 |s_{\theta\delta} + \eta_{\theta\alpha,l} + f_l^2|, \quad (14)$$

with

$$f_l^2 = \frac{\sigma_\phi^2}{\sigma_\phi^2} \frac{\sum_m A_{l,m} \theta_m \sum_{m'} A_{l,m'} \delta_{m'}}{\sum_m A_{l,m}^2}, \quad (15)$$

where  $s_{\theta\delta}$  measures the spatial covariance between  $\theta_m$  and  $\delta_m$ , and  $f_l^2$  is a lead-dependent factor weighted by  $\sigma_\phi^2$ .

There are a few issues that limit the possibility of using the difference of  $\mathcal{V}$ -index in even and odd beats as estimator of  $s_{\theta\delta}$ . First, the difference in  $v_{2i,l}^2$  and  $v_{2i-1,l}^2$  is not only proportional to  $s_{\theta\delta}$ . In particular, the term  $f_l^2$  is proportional to the variance  $\sigma_\phi^2$ , which could be potentially increased by little bracketing errors (*i.e.*, errors in the detection of fiducial points) of the T-waves composing the set of beats (recall that the reference time point is assumed to be the same for all beats). Second,  $f_l^2$  is also proportional to  $\sum_m A_{l,m} \theta_m$ , which is equivalent to the expected value of the lead factor  $w_1$ . This term is known to be the largest among all lead factors [16] and in computerized simulations using the ESS model implemented using ECGSIM (see Section III-A) we found that  $f_l^2$  was up to 60 times larger than  $s_{\theta\delta}$ . Third, a model fitting algorithm would require to impose a common DTW for all (even and odd) beats, as explained above. However, the beat-to-beat time shift (*e.g.*, due to the effect of  $\bar{\delta}$ ) of the APs would lead to a single  $t_d(t)$  wave which is a sort of mixture of the two even and odd DTWs. This mixture would require more higher-order terms in the Taylor's expansion to compensate for the shift and fit the two beats, but higher-order derivatives of DTW are numerically challenging to estimate.

In order to tackle the above mentioned issues, and similarly to what originally proposed for the  $\mathcal{V}$ -index, we reformulate the

surface ECG model by changing the time point for the Taylor's expansion of  $d(t)$ , *i.e.*, the average repolarization time of each beat  $\bar{\rho}_k$  instead of  $\bar{\rho}$ , as follows

$$\begin{aligned} d(t - \rho_{k,m}) &\approx d(t - \bar{\rho}_k) \\ &\quad - \dot{d}(t - \bar{\rho}_k) \left[ \theta_m + \phi_{k,m} + (-1)^k \frac{\delta_m}{2} \right] \\ &\quad + \frac{1}{2} \ddot{d}(t - \bar{\rho}_k) \left[ \theta_m + \phi_{k,m} + (-1)^k \frac{\delta_m}{2} \right]^2. \end{aligned} \quad (16)$$

Consequently, the surface ECG model becomes

$$\begin{aligned} \psi_k(t) &\approx \mathbf{w}_{1,k} t_{d,k}(t) + \mathbf{w}_{2,k} \dot{t}_{d,k}(t) \\ \mathbf{w}_{1,k} &= -\mathbf{A} \left[ \boldsymbol{\theta} + \boldsymbol{\phi}_k + (-1)^k \frac{\boldsymbol{\delta}}{2} \right] \\ \mathbf{w}_{2,k} &= \frac{1}{2} \mathbf{A} \left[ \left( \boldsymbol{\theta} + \boldsymbol{\phi}_k + (-1)^k \frac{\boldsymbol{\delta}}{2} \right) \circ \left( \boldsymbol{\theta} + \boldsymbol{\phi}_k + (-1)^k \frac{\boldsymbol{\delta}}{2} \right) \right] \end{aligned} \quad (17)$$

where  $t_{d,k}(t) = \dot{d}(t - \bar{\rho}_k)$ ,  $\mathbf{w}_{k,1}$  and  $\mathbf{w}_{k,2}$  are the lead factors, and  $\boldsymbol{\delta}$  is an  $M$  dimensional vector containing all  $\delta_m$  values. Note that the dependency on  $k$  is explicitly introduced in  $t_{d,k}(t)$  to account for different DTWs (for instance, due to temporal shifts) between even and odd beats.

Similarly to (14), lead factors can be used to compute the difference between  $\mathcal{V}$ -index of even and odd beats, obtaining

$$|v_{2i,l}^2 - v_{2i-1,l}^2| = 2 |s_{\theta\delta} + \eta_{\theta\delta,l}| \approx 2 |s_{\theta\delta}|, \quad (18)$$

where  $s_{\theta\delta}$  measures the spatial covariance between  $\theta_m$  and  $\delta_m$  (see Appendix [17]). The new formulation makes (18) not dependent on the  $f_l^2$  term, but makes the model insensitive to the global alternans  $\bar{\delta}$ . Note that in (14),  $\eta_{\theta\alpha,l}$  appears rather than  $\eta_{\theta\delta,l}$  as in (18). The model in (17) can be fitted on each T-wave independently because no constrains on the DTW morphology are set (for instance, no alignment of T-waves is needed). Note that, for simplicity, same notation is used in (18) and (14) for the  $v_k$  values, but they are computed differently, in (14) a unique DTW is used in the calculations, while in (18) a DTW is used for each beat, allowing to get rid of the terms  $\sigma_\phi^2$  and  $\bar{\delta}$ .

Given the fact that repolarization alternans was found associated with increased spatial dispersion of ventricular repolarization [7], it is sensible to normalize the quantity in (18) with the value of  $\mathcal{V}$ -index i) to reduce the effect of the dispersion of ventricular repolarization (estimated by the  $\mathcal{V}$ -index) when the index is used for cardiac risk assessment; and ii) to compensate for the inter-subject variability by accounting for different basal levels of heterogeneity since ventricular repolarization is known to be a subject-dependent phenomenon. During alternans, we thus define the  $\mathcal{V}$ -index of a set of beats as its average on even and odd beats, which, making use of derivations in Appendix [17],

results in,

$$\begin{aligned} & \frac{v_{2i,l}^2}{2} + \frac{v_{2i-1,l}^2}{2} \\ &= \frac{\sigma_\phi^2}{2} + s_{\theta\theta} + \frac{s_{\delta\delta}}{4} + \eta_{\theta\theta,l} + \frac{\eta_{\delta\delta,l}}{4}. \end{aligned} \quad (19)$$

We now introduce the lead-dependent ratio,  $r_l$ , for lead  $l$ ,

$$r_l = \frac{1}{2} \frac{v_{2i,l}^2 - v_{2i-1,l}^2}{\sqrt{\frac{v_{2i,l}^2}{2} + \frac{v_{2i-1,l}^2}{2}}}, \quad (20)$$

as the quotient of (18) and the square root of (19) (resulting in a quantity measured in ms). Taking the average of the ratios  $r_l$  along leads, we introduce a new metric, named  $\mathcal{R}$  index, which is approximately proportional to the product of the standard deviation of the alternans  $\delta_m$  and the Pearson's correlation coefficient  $p_{\theta\delta}$ , as

$$\mathcal{R} = \left| \frac{1}{L} \sum_{l=1}^L r_l \right| \approx |p_{\theta\delta} \sqrt{s_{\delta\delta}}|, \quad (21)$$

also measured in ms. In practice, the estimates  $\hat{\mathcal{R}}$  and  $\hat{r}_l$  of  $\mathcal{R}$  and  $r_l$  are obtained using  $\hat{v}_{2i,l}^2$  and  $\hat{v}_{2i-1,l}^2$ , as computed in the context of (8), but with DTW estimated at each beat as described in (16), and then used in (20) and (21).

### F. Estimate of $\bar{\delta}$

The model in (17) does not capture changes in  $\bar{\delta}$ . However, this quantity is relevant for characterizing repolarization alternans. We thus propose a crosscorrelation-based algorithm for its quantification using the set of DTWs already computed. The algorithm consists of three steps: i) T-wave bracketing; ii) time delay estimation between DTWs; iii) computation of  $\bar{\delta}$  and, as a by-product,  $\sigma_\phi^2$ .

First, given the fact that estimating  $\bar{\delta}$  requires a common time reference across beats, T-wave bracketing is performed by extracting a time window starting from the Q onset +150 ms of each beat and spanning enough to cover all T-waves.

Second, during alternans, two families of DTWs are possibly expected to be available, corresponding to even and odd beats, respectively. For each family, Woody's algorithm [20] is used to align all DTWs and create an average DTW template. The intra-delays estimated from each DTW are estimates of  $\bar{\phi}_k$ , whereas  $\sigma_\phi^2$  can be then quantified by considering all intra-delays of even and odd beats together and computing their variance. Third, the absolute value of the time delay between the two templates, computed via crosscorrelation, is an estimate of  $\bar{\delta}$ .

We denote as  $\hat{\bar{\delta}}$  and  $\hat{\sigma}_\phi$  the estimates of  $\bar{\delta}$  and  $\sigma_\phi$ , respectively.

### G. TWA Assessment

TWA was computed from the vector magnitude<sup>2</sup> of the surface T-wave using the algorithm proposed in [2]. Briefly, the difference between consecutive T-waves was first calculated and the sign of the residual was adjusted considering the beat-to-beat

alternans assumption. We then computed the median alternans waveform and finally TWA was quantified as the root mean square of such median wave.

## III. DATA

### A. Computerized Simulations

The estimates of  $\mathcal{R}$  index and  $\bar{\delta}$  were tested by means of a Matlab code transposition (R2020b, The MathWorks, Inc.) of the free software ECGSIM [21]. The software implemented the ESS model in (1) to generate the surface ECG from the myocytes' APs.

In our simulations, the ECGSIM model had  $M = 257$  nodes. The standard deviation of the repolarization times provided by ECGSIM was  $\sqrt{s_{\theta\theta}} = 33.20$  ms. APs were generated using a product of logistic functions as in [16].

Synthetic ECG segments with 128 beats were generated.  $\phi_{k,m}$  values were extracted from a zero-mean normal distribution with  $\sigma_\phi = 1$  ms [16]. The lead factors  $w_{1,k}$  and  $w_{2,k}$  were estimated using an iterative procedure for each  $k$ -th beat (see Section III-B3 for further details). Unless differently specified,  $\sigma_{\bar{\phi}}$  was estimated recalling that in our model, the variability of repolarization times is given by  $\phi_{k,m}$  and  $\bar{\phi}_k$  and that the QT variability at rest is about 5 ms [19], we therefore set  $\sigma_{\bar{\phi}}^2 + \sigma_\phi^2 = 5^2 \text{ ms}^2$ , implying setting  $\sigma_{\bar{\phi}} = \sqrt{24}$  ms.

Three sets of computerized simulations were performed:

1) **Sensitivity Analysis:** We assessed how repolarization alternans affected the surface ECG using a stochastic model for  $a_m$ . In particular, we quantified the effect produced by  $s_{\delta\delta}$ ,  $\bar{\delta}$  and the correlation  $p_{\theta\delta}$  between  $\theta_m$  and  $\delta_m$ . To do so,  $a_m$  was set as follows

$$\begin{aligned} a_m &= \bar{\delta} + \delta_m \\ &= \bar{\delta} + \alpha p_{\theta\delta} \theta_m + \alpha \sqrt{(1 - p_{\theta\delta}^2) s_{\theta\theta} z_m} \end{aligned} \quad (22)$$

where  $z_m$  are values extracted from a standard Normal distribution,  $\alpha$  sets the spatial variance of  $\delta_m$ , *i.e.*,  $s_{\delta\delta} = \alpha^2 s_{\theta\theta}$ . The global alternans  $\bar{\delta}$  was varied between 0 to 20 ms,  $\alpha$  from 0 to 0.4 (40% of the spatial dispersion  $\sqrt{s_{\theta\theta}}$ ), and  $p_{\theta\delta}$  between 0 to 1. Values of  $\hat{\mathcal{R}}$  were computed for each combination of these three parameters. In addition, we quantified the  $\eta_{\delta\delta,l}$ ,  $\eta_{\theta\delta,l}$  and  $f_l^2$  terms to assess their magnitude with respect to  $s_{\theta\delta}$  and  $s_{\delta\delta}$ . The  $L$  values of  $\eta_{\delta\delta,l}$ ,  $\eta_{\theta\delta,l}$  and  $f_l^2$  terms were first averaged and then their absolute value was computed.

The errors of the estimates of  $\hat{\bar{\delta}}$  with respect to their corresponding true values were also computed. In this case, 100 random samplings were performed for the three parameters  $s_{\delta\delta}$ ,  $\bar{\delta}$  and  $p_{\theta\delta}$  in the same aforementioned ranges and for  $\sigma_{\bar{\phi}}$  between 0 and 5 ms.

2) **Regional Alternans:** We investigated the role of repolarization alternans affecting a single ventricular region on both TWA and  $\hat{\mathcal{R}}$ . The simulation setting was inspired by the one presented in [10]. It considered 7 different regions separately, *i.e.*, apical left ventricle, apical right ventricle, lateral left ventricle, lateral right ventricle, basal left ventricle, basal right ventricle,

<sup>2</sup>Vector magnitude is the square root of the sum of the squared ECG leads.

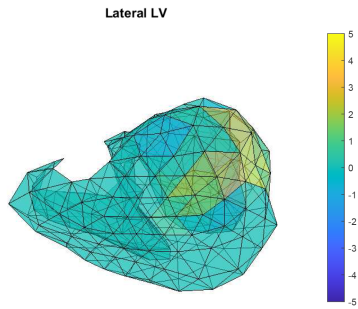


**Fig. 1.** Example of alternans distribution  $a_m$  for lateral LV region. The region covered approximately 30% of the total ventricular surface. The color represents the alternans of the repolarization time, reported in ms, for each node  $m$  in the model. The central node of each region was set to have the largest alternans (in this case, 5 ms), while the other nodes within the regions progressively reduced their alternans to reach 0 ms at the boundary.

and apical center, with a size varying between 10% and 90% (step 10%) of the total ventricular surface.

The central node  $m^*$  of the region was set to have an alternans of  $a_{m^*} = 0.7 \times \theta_{m^*}$  ms. The alternans of the other nodes were set to  $a_m = c_m \theta_{m^*}$  with the coefficient  $c_m$  linearly dependent to the distance between the central node  $c_{m^*} = 0.7$  and the boundary of the region  $c_m = 0$ . Nodes on the region boundary had no alternans. **Fig. 1** shows an example of alternans distribution for this simulation setup.

**3) Noise-Sensitivity Analysis:** We assessed the impact of the noise on the estimates of  $\mathcal{R}$  index and  $\bar{\delta}$ . To do that, the approach described in [22] was followed and adapted for our scenario. Briefly, the MIT-BIH Noise Stress Test Database [23] was downloaded from Physionet [24]. The database contains 2-lead recordings of three types of noise, *i.e.*, baseline wander, muscle artifact and electrode motion artifact. The noise was added to T-waves generated using the ECGSIM software at different levels of signal-to-noise-ratios (SNRs), ranging from 5 to 30 db. The average variance across leads was retained as reference of the signal power. One hundred twenty eight T-waves were generated for each of the following 4 settings: i) no alternans ( $\alpha = 0$  and  $\bar{\delta} = 0$  ms); ii) only global alternans ( $\bar{\delta} = 10$  ms); iii) only spatial alternans ( $\alpha = 0.2$  and  $p_{\theta\delta} = 0.7$ ); and iv) both spatial alternans and global alternans ( $\alpha = 0.2$ ,  $p_{\theta\delta} = 0.7$  and  $\bar{\delta} = 10$  ms).

As described in [22], the number of leads for the noisy recordings had to be augmented to match the desired dimension, that, in our case, was the one of the simulated T-waves. Such augmentation was performed by means of a resampling technique of the original 2-lead recordings. For each of the 12 leads of the simulated T-waves, from the 2-lead recordings, a random lead  $l$  between the first and second lead and a random time instant  $t$  were extracted: a time window on the lead  $l$ , starting from the time instant  $t$ , of the same size of the T-wave, was then considered to be added to the simulated T-wave.

The resampling technique does not retain the noise correlation across leads, which is instead known to be present. In order to include a realistic noise correlation in our simulations, we considered the ECG noise collected from one subject. In

particular, a random subject of the STAFF-III dataset (see Section III-B) was selected and the ECG in baseline was further processed. The TQ track was extracted and the correlation matrix  $C$  of the noise was computed. The Cholesky decomposition was derived from  $C$  to obtain the whitening matrix  $D$ . The inverse of  $D$  was applied to 12-lead noise matrix to enforce the realistic correlation. The application of  $D$  was performed after normalizing the variance of each of the 12 leads to  $1 \text{ mV}^2$ . The approach was described in [22].

The procedure was repeated 100 times for each type of noise by resampling the noisy signals.

## B. STAFF-III Dataset

Percutaneous transluminal coronary angioplasty (PTCA) is a surgical procedure meant to open up blocked coronary arteries and restore the normal blood flow. PTCA represents one of the possible treatments for myocardial ischemia or infarction. It involves the insertion of an inflatable balloon inside the coronary artery that is repeatedly inflated and deflated to facilitate the blood to flow.

In addition to the clinical relevance of such procedure, PTCA provides an excellent model to investigate the electrophysiological changes of early-stage ischemia. Indeed, the complete coronary occlusion caused by balloon angioplasty allows to study the first minutes of the ischemic process [25].

We computed the  $\hat{\mathcal{R}}$  and  $\hat{\bar{\delta}}$  on the STAFF-III dataset, freely available from PhysioNet [26], [27], [28], in which subjects underwent to PTCA using prolonged (4-min average) balloon inflations. The main reason behind the selection of this dataset was that it contained subjects in which TWA has been observed and quantified on the surface ECG [2].

**1) Study Population:** The STAFF-III dataset consisted in 104 patients that underwent PTCA using prolonged balloon inflations. During the surgical procedure, a standard 9-lead ECG was recorded (V1, V2, V3, V4, V5, V6, I, II, III). The augmented leads were then mathematically generated. ECGs had a resolution of  $0.625 \mu\text{V}$  and were acquired with a sampling rate of 1000 Hz.

The clinical protocol was divided into three phases as follows. First, before any catheter insertion, a baseline pre-inflation 5-min ECG was acquired at rest in either a relaxing room or catheterization laboratory (CathLab), or both. Second, PTCA was performed and the ECG of up to 5 consecutive inflations was recorded. The inflation time was also annotated. Third, post-inflation ECGs were acquired for 5 min at rest in either a relaxing room or in the catheterization laboratory, or both. The dataset did not contain patients suffering from ventricular tachycardia, undergoing an emergency procedure, or displaying signal loss during acquisition.

As dye injections applied during PTCA may alter the ECG morphologies, injection times were carefully annotated and provided within the dataset. For further clinical details, please refer to [26], [28].

**2) ECG Preprocessing and Selection of Segments:** ECG segments of 128 beats with a 50% overlap were preprocessed using a Butterworth filter (3rd-order, zero-phase, 0.5-15 Hz)

to reduce powerline interference, baseline wandering and high frequency noise, while maintaining the alternans components as in [3]. After filtering, the baseline of all signals was adjusted to set the isoelectric segment back to 0 mV using the algorithm reported in [29].

The quality of the leads in each segment was determined as the average crosscorrelation between a mean QRS template and each QRS complex. A lead was considered of sufficient quality when such average was higher than 0.9 [29]. Segments were discarded from the analysis if less than three leads of good quality were available.

Afterwards, ECG segments were defined as eligible for being further analyzed only if its HR was considered stable. We used the following rules: i) the difference between the maximum and the minimum instantaneous HR during the segment was 20 beats/min; ii) at least 80% of the beats were labeled as normal sinus beat with a difference between consecutive RR intervals lower than 150 ms. Since ectopic beats or unstable HR might change the morphology of the T-wave, whenever a beat was rejected, both previous and next beats were excluded as well. The segment selection strategy was similar to the one presented in [3].

For each valid ECG segment, T-waves were segmented by considering a fixed time window for all the beats. The time window started 100 ms after the R-peak and ended 20 ms after the median end of the T-waves. T-wave end points were determined using the Surawicz method [30] applied on the vector magnitude of the average beat.

**3) Estimation of the  $\mathcal{R}$  Index:** The lead factors  $w_{k,1}$  and  $w_{k,2}$  and DTWs were estimated for each valid T-wave within a stable ECG segment. We used the iterative algorithm reported in [16] to minimize the mean square error between the ECG leads and the model  $w_{k,1}t_{d,k}(t) + w_{k,2}\dot{t}_{d,k}(t)$ , built using two terms of the Taylor expansion. Briefly, the algorithm splits the problem into two subproblems solved iteratively. First, an estimate of  $t_{d,k}(t)$  is obtained, then the lead factors can be computed by considering  $t_{d,k}(t)$  as known. The procedure is then repeated until convergence or a certain number of iterations. The algorithm has been already validated on several other datasets (*e.g.*, [29], [31], [32]) and proved to be sensitive to the dispersion of the ventricular repolarization.

A model fitting rejection procedure was used afterwards to exclude those beats whose DTW was correlated less than 0.9 with the median DTW template. This procedure was meant to remove beats in which the model fitting went likely wrong.

Once the lead factors were determined, we computed the  $\hat{\mathcal{R}}$  using the estimate of (21). To summarize, the lead factors included in the computation were only those belonging to normal sinus beats with stable HR and not discarded by the model fitting rejection procedure.

**4) TWA Measurement:** We quantified TWA on the STAFF-III using the algorithm reported and validated on the same dataset by Martínez et al. [2]. They showed that the algorithm detected TWA from a few microvolts up to several hundreds of microvolts during balloon inflation. The algorithm is described in Section II-G. Differently from simulations, the estimation was repeated

for each ECG lead and their maximum value was retained, as reported in [2].

### C. Experimental and Statistical Analyses

In this study, we focused our analyses on a subset of the STAFF-III dataset. Specifically, we considered only ECGs collected during baseline (pre-operation), first inflation and post-inflation (post-operation), respectively.

Similar to [2], the time evolution of the  $\hat{\mathcal{R}}$  index,  $\hat{\delta}$  and  $\hat{\sigma}_{\bar{\phi}}^2$  was quantified from the beginning of the first inflation up to either the end of it or the dye injection, as well as during pre- and post-operation. The Wilcoxon signed rank test (significance at  $p < 0.05$ ) was applied to test the effect of the inflation during the first and fourth minutes with respect to pre-operation, and pre- vs post-operation, in terms of  $\hat{\mathcal{R}}$  index. In addition, the Pearson's correlation coefficient was determined between  $\hat{\mathcal{R}}$  and TWA at pre-operation, and at the last part of the inflation (fourth minute), respectively.

## IV. RESULTS

### A. Computerized Simulations

**1) Sensitivity Analysis:** On synthetic data, we observed a positive gradient of TWA with respect to  $\bar{\delta}$  and  $s_{\delta\delta}$  (Fig. 2(a), 2(b) and 2(c)). No TWA was measured when  $\bar{\delta} \approx 0$  ms and  $\sqrt{s_{\delta\delta}} \approx 0$  ms (Fig. 2(a) and 2(b)), while large values of both quantities resulted in TWA of a few hundreds of microvolt.

The coefficient  $p_{\theta\delta}$  was positively correlated with TWA (Fig. 2(b) and 2(c)). This result was visible for both  $\bar{\delta} = 0$  ms (Fig. 2(b)) and  $\bar{\delta} = 10$  ms (Fig. 2(c)). High values of both  $p_{\theta\delta}$  and  $s_{\delta\delta}$  produced a large increase in TWA (top right corners of Fig. 2(b) and 2(c)). In addition, the effect of  $p_{\theta\delta}$  when combined with  $\bar{\delta} > 0$  was found to increase TWA. This can be observed in Fig. 2(a), when  $\bar{\delta} = 10$  ms, reports a TWA about 100  $\mu\text{V}$  (here,  $p_{\theta\delta} = 0$ ), equivalently to the bottom row of Fig. 2(c), while all other values of the third panel ( $p_{\theta\delta} > 0$ ) show TWA higher than 100  $\mu\text{V}$ .

The  $\hat{\mathcal{R}}$  index behaved differently. First, no correlation was found between  $\hat{\mathcal{R}}$  and  $\bar{\delta}$ , regardless the values of  $s_{\delta\delta}$  when  $p_{\theta\delta} = 0$  (Fig. 2(d)). Second, positive correlations were found between  $\hat{\mathcal{R}}$  and both  $p_{\theta\delta}$  and  $s_{\delta\delta}$  (Fig. 2(e)). The same pattern was found when combining the effect of  $\bar{\delta}$  and  $p_{\theta\delta}$ , showing that  $\bar{\delta}$  did not play a substantial role in the index (Fig. 2(e) vs 2(f)). These results were as expected according to (21).

The cross-lead average values of  $\eta_{\theta\delta,l}$  and  $f_l^2$  are reported in Fig. 2(g) and 2(h), respectively. The trend of  $\eta_{\theta\delta,l}$  follows the one of Fig. 2(g) with halved values approximately. All values were found to increase with  $p_{\theta\delta}$  and  $s_{\delta\delta}$ . Both  $\eta_{\theta\delta,l}$  and  $\eta_{\delta\delta,l}$  were negligible for the  $\mathcal{R}$  index while varying  $p_{\theta\delta}$  and  $s_{\delta\delta}$ . Indeed,  $\eta_{\theta\delta}/s_{\theta\delta}$  and  $\eta_{\delta\delta}/s_{\delta\delta}$  were found  $\ll 1$ . On the other hand,  $f^2$  was very large and not negligible with respect to  $s_{\theta\delta}$ .

The values of  $\hat{\delta}$  and  $\hat{\sigma}_{\bar{\phi}}$  were found highly correlated with the true  $\bar{\delta}$  and  $\sigma_{\bar{\phi}}$  (Fig. 3(a) and 3(b)). In particular, the former achieved high precision when repolarization alternans was modeled with only  $\bar{\delta}$  (red dots in Fig. 3(a)), suggesting that the global

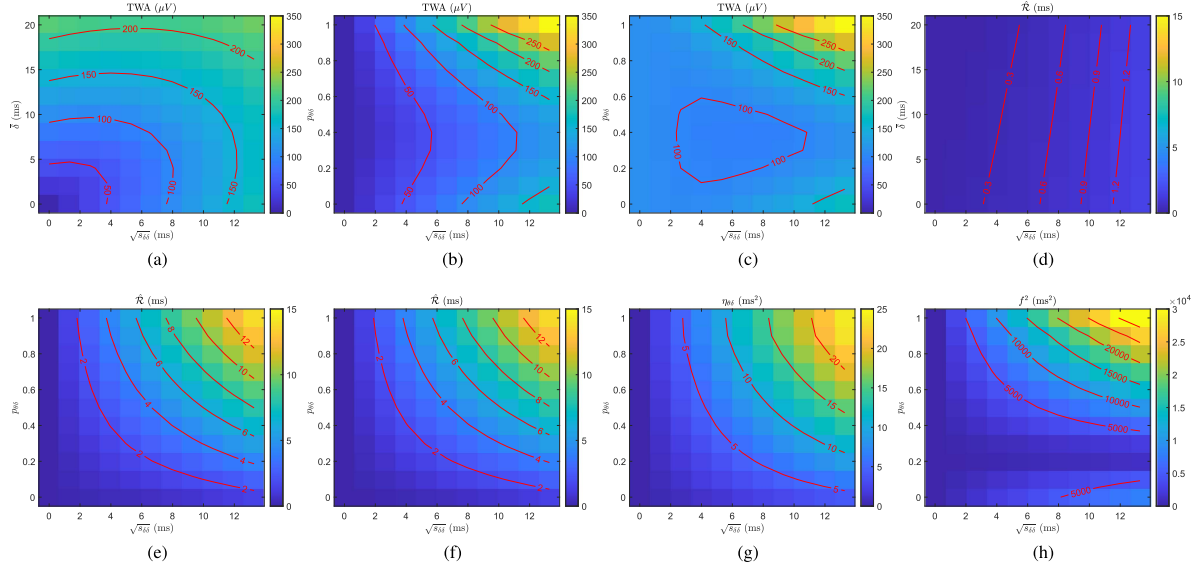


**Fig. 2.** Results of the first computerized simulation. TWA ( $\mu\text{V}$ ) and  $\hat{\mathcal{R}}$  (ms) values were computed while varying  $\bar{\delta}$  (ms),  $\sqrt{s_{\delta\delta}}$  (ms) and  $p_{\theta\delta}$ . Panels (a) and (d) report results from simulations in which the spatial correlation  $p_{\theta\delta}$  was set to 0, while  $\bar{\delta}$  and  $s_{\delta\delta}$  varied. Panels (b) and (e) depict the values of the two indexes as function of  $s_{\delta\delta}$  and  $p_{\theta\delta}$ , while keeping  $\bar{\delta} = 0$  ms. Finally, panels (c) and (f) show the results as in (b) and (e), respectively, but with  $\bar{\delta} = 10$  ms. The last two panels report the values of  $\eta_{\theta\delta}$  (g) and  $f^2$  (h).  $\eta_{\theta\delta}$  follows the same trend of (g) with values approximately halved. For visualization purpose, these values were first averaged across leads (they are indeed lead-dependent) and then their absolute value was computed.

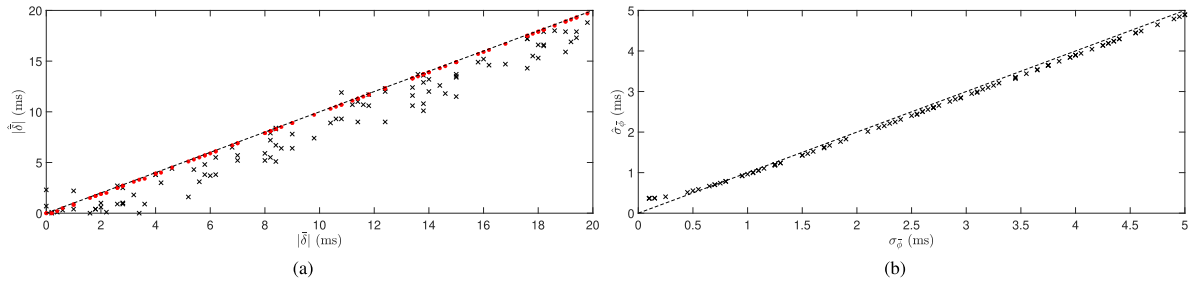


**Fig. 3.** Scatter plot of true and estimated values for  $\bar{\delta}$  (a) and  $\sigma_{\bar{\delta}}$  (b) for 100 random sampling of  $\bar{\delta}$ ,  $p_{\theta\delta}$  and  $s_{\delta\delta}$ . Red dots in (a) correspond to the same sampling but with  $\sqrt{s_{\delta\delta}} = 0$  ms (*i.e.*, only the global alternans  $\bar{\delta}$  was present in the simulations).

**TABLE I**

$R^2$  COEFFICIENTS FOR REGIONAL ALTERNANS SIMULATION RESULTS BETWEEN TWA,  $\hat{\mathcal{R}}$ ,  $p_{\theta\delta}$ ,  $\sqrt{s_{\delta\delta}}$  AND REGION SIZE POOLED TOGETHER. ALL CORRELATIONS WERE FOUND STATISTICALLY SIGNIFICANTLY DIFFERENT THAN ZERO ( $p < 0.05$ )

	$ p_{\theta\delta} $	$\sqrt{s_{\delta\delta}}$	$ p_{\theta\delta}\sqrt{s_{\delta\delta}} $	Reg. size
TWA	0.35	0.20	0.24	0.27
$\hat{\mathcal{R}}$	0.73	0.63	0.74	0.69
$ p_{\theta\delta} $	—	—	—	0.84
$\sqrt{s_{\delta\delta}}$	—	—	—	0.70

All correlations were found statistically sign than zero ( $p < 0.05$ )

alternans can be estimated by looking at the time delay between DTWs of even and odd beats. On the other hand, when  $\delta_m$  was also present, the performance of the algorithm decreased due to the change in morphology of DTWs.

**2) Regional Alternans:** Table I and Fig. 4 report a summary of the results for the simulation of regional alternans. We found that both TWA and  $\hat{\mathcal{R}}$  index increased with  $|p_{\theta\delta}\sqrt{s_{\delta\delta}}|$  across all simulations results pooled together, with the former having

a larger relative variance and site dependence. Similar results were obtained when correlating the two indexes with  $|p_{\theta\delta}|$  and  $\sqrt{s_{\delta\delta}}$  separately (Table I).

The relationship between region size and the indexes followed a similar pattern (Table I). In particular, TWA was found moderately correlated to the region size while  $\hat{\mathcal{R}}$  was found highly correlated, mainly due to the high correlation between region size and  $|p_{\theta\delta}|$ . In addition, the larger the region size, the larger  $s_{\delta\delta}$ .

**3) Noise-Sensitivity Analysis:** Fig. 5 reports the results of the noise-sensitivity analysis.

As expected, the errors between the indexes and references (boxplots and red dashed lines in Fig. 5, respectively), and standard deviations of both estimates of  $\mathcal{R}$  and  $\bar{\delta}$  reduced when the SNR was increased (all panels in Fig. 5). The  $\hat{\mathcal{R}}$  values were found having a bias with respect to the reference  $p_{\theta\delta}\sqrt{s_{\delta\delta}}$  used. This result was expected since the  $\mathcal{R}$  index defined in (21) differs from the reference by a quantity depending to  $\eta_{\theta\delta,l}$ ,  $\eta_{\delta\delta,l}$  and  $\eta_{\theta\delta,l}$  (Fig. 5(a), (c), (e), (g)). In addition, the bias was higher in presence of spatial alternans with respect to only global alternans (Fig. 5(c) vs 5(e)) and further increased in combination of the two (Fig. 5(c) and 5(e) vs 5(g)).



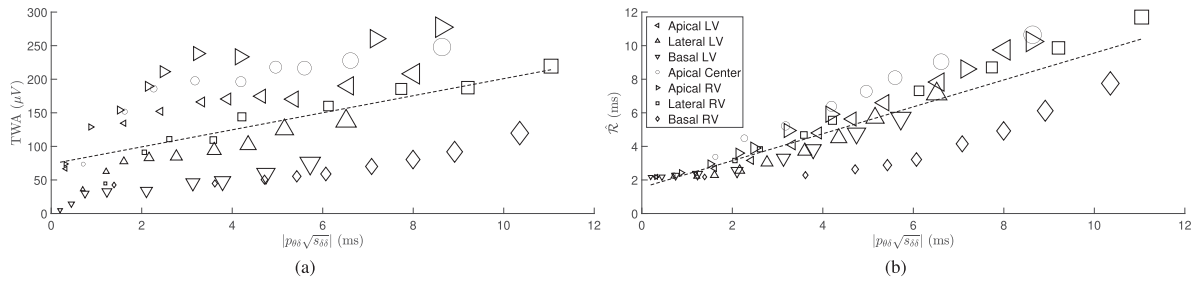


Fig. 4. Results of the regional alternans simulation. In particular, scatterplots between the  $|p_{\theta\delta}\sqrt{s_{\delta\delta}}|$  and both TWA (a) and  $\hat{R}$  index (b) are reported. TWA was estimated on the VM. The linear regression line is depicted with dashes. Marker sizes are proportional to the region dimension.

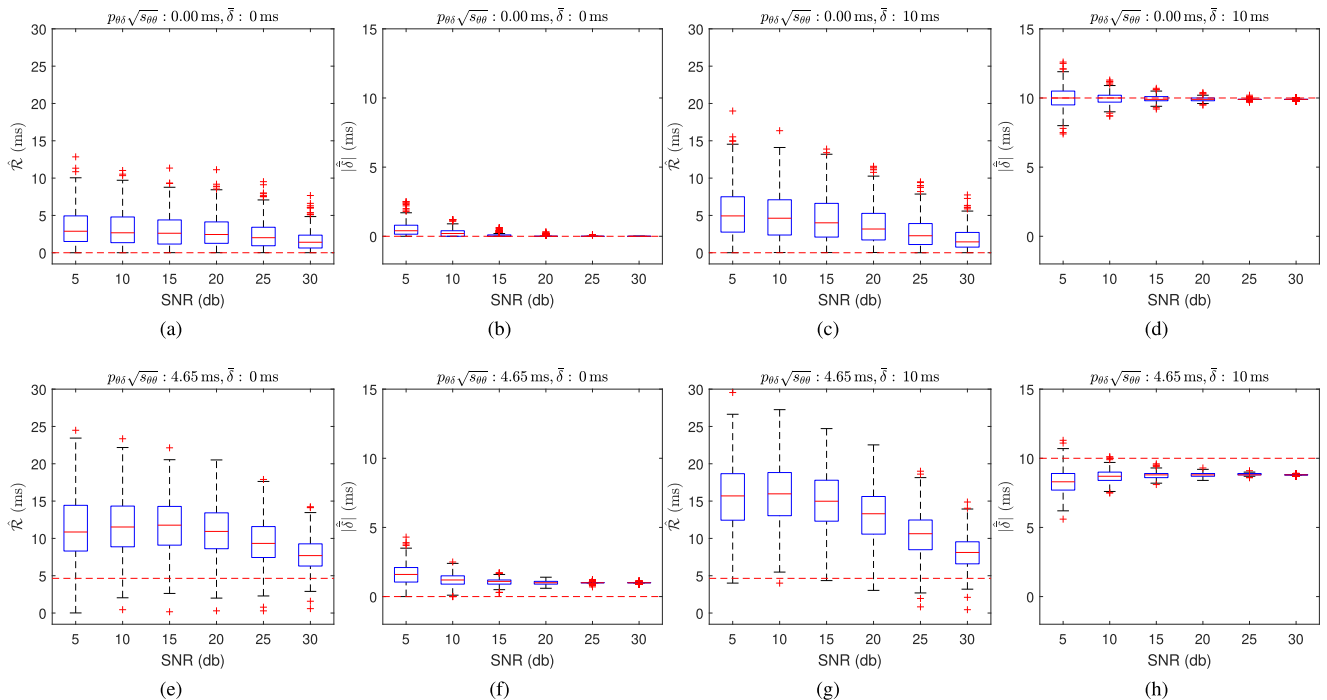


Fig. 5. Boxplot of  $\hat{R}$  index and  $\hat{\delta}$  values for the results of the noise-sensitivity analysis for different SNRs. Boxplots contain 300 values, *i.e.*, 100 per each noise type. Red dashed lines represent the reference level for the specific simulation.

Similar to the results obtained in the Sensitivity analysis, the estimate of  $\bar{\delta}$  was found close to the reference value when no spatial alternans was in place, while a bias was observed when present (Fig. 5(b) and 5(d) vs 5(f) and 5(h)). This result was observed in Fig. 3 as well.

Errors and standard deviations were found similar across the three different types of noise (data not shown).

### B. STAFF-III Dataset Results

Both TWA and  $\hat{R}$  index were able to track the time course of the inflation and showed a progressive increase from the first minute up to the fourth one (Fig. 6(a) and 6(b)). Focusing on the  $\hat{R}$  index, a statistically significant difference was found between the fourth minute and pre-operation ( $\Delta\hat{R}$ : median 0.81 IQR (-0.25, 6.38) ms;  $p < 0.05$ ), whereas no differences were found either between pre-operation and first minute, or between pre- vs post-operation ( $p > 0.05$ ). The increase was not due to change

in RR values during inflation (known to occur [2]) with respect to pre-operation. Indeed, the Pearson's correlation coefficient between the  $\hat{R}$  with RR values during pre-operation was not statistically significantly different from zero ( $p > 0.05$ ). Also, no correlation was found between TWA and the  $\hat{R}$  index during pre-operation, whereas a moderate significant correlation was found during the fourth minute (Pearson's correlation coefficient of 0.49;  $p < 0.05$ ). Fig. 6(a) and 6(b) report the time course of TWA and  $\hat{R}$  index, respectively.

Estimates of  $\sigma_{\bar{\phi}}$  and  $\bar{\delta}$  were also obtained. The time course of the former is reported in Fig. 6(c). With respect to pre-operation values, an abrupt change in  $\hat{\sigma}_{\bar{\phi}}$  was visible during the first minute of inflation (median 2.20 IQR (0.77, 3.97) ms;  $p < 0.05$ ) while a progressive reduction was observed during the next minutes, reaching pre-operation values. Regarding  $|\hat{\delta}|$ , most values estimated were 0 ms within all protocol phases with some rare exceptions during the fourth minute.

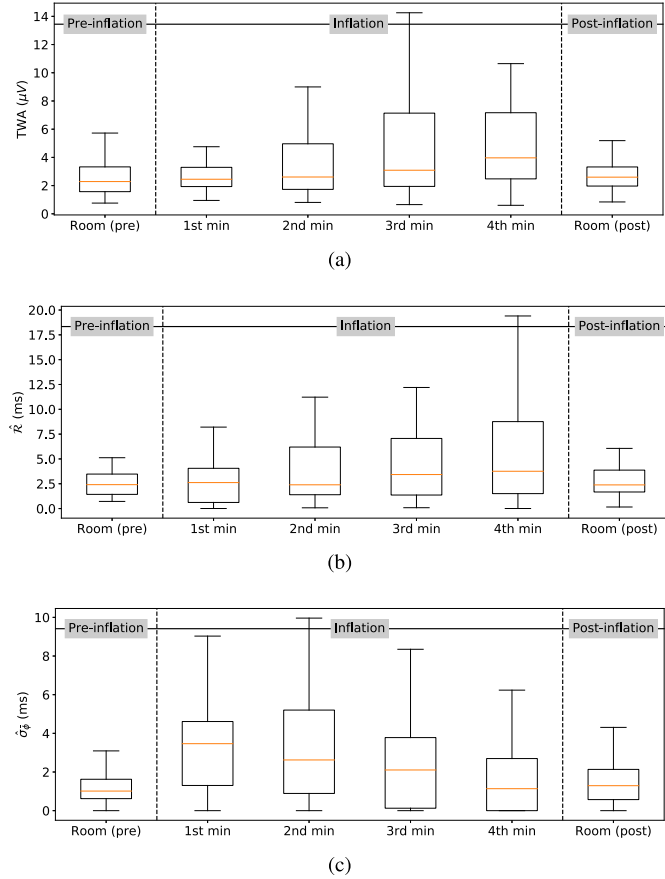


Fig. 6. Time course of TWA (a),  $\hat{\mathcal{R}}$  (b) and  $\hat{\sigma}_{\bar{\phi}}$  (c). Outliers are not reported for visualization purpose.

## V. DISCUSSION

In the first part of the work, we introduced a new model for repolarization alternans and assessed how it reflects on the surface ECG in terms of TWA. According to (13), the expected value of TWA on the surface ECG depends on four main factors. The first one is the spatial alternans distribution  $\delta_m$ , the second one is the transfer matrix  $\mathbf{A}$ , that encodes the geometry, volume conductor and lead placement, the third one is the shape of the AP (encoded in the DTW), and the fourth one is the product between the repolarization time delay of each node and its alternating component  $\theta_m(\bar{\delta} + \delta_m)$  (weighted by the transfer matrix  $\mathbf{A}$ ). Regarding the last factor, TWA is amplified when the product is large or, in other words, when the spatial covariance between the repolarization time delay  $\theta_m$  and the alternans  $\delta_m$  reaches high values. The results were also observed in computerized simulations (Fig. 2(b) and 2(c)), where TWA measured on the surface ECG changed from few microvolts to a few hundreds when increasing the correlation between  $\theta_m$  and  $\delta_m$ . The effect of their product on TWA becomes observable after introducing the second order approximation of the surface ECG through the lead factor  $w_{2,k}$  (in a previous work, only the first lead factor was used in the approximation, that made such effect not visible [33]).

Our results are in line with the work of Choi and Salama [6] in which guinea-pig hearts displayed a moderate-to-high correlation ( $\approx 0.7$ ) between action potential duration and repolarization alternans  $\delta_m$ , suggesting that what is observed on the surface ECG might be dependent on such correlation. In addition, despite the fact that the model proposed cannot explain the ion channel mechanisms responsible for existence of the spatial covariance between  $\theta_m$  and  $\delta_m$ , Choi and Salama [6] observed that, during alternans, the intracellular calcium concentration (specifically  $\text{Ca}_i^{2+}$ ) showed alternations too. It is also well known that abnormal calcium handling tends to increase the heterogeneity of ventricular repolarization [34], thus making such ion channel the main possible responsible for the increase of both  $s_{\theta\theta}$  and  $s_{\delta\delta}$ .

In the second part of the work, we derived a new index, *i.e.*, the  $\hat{\mathcal{R}}$  index, whose numerator was found to be selectively sensitive to the covariance between  $\theta_m$  and  $\delta_m$ , and proposed an algorithm for estimating the global alternans  $\bar{\delta}$ .

The index was first tested on computerized simulations with three different simulation settings. The common outcome of the first two simulations was the sensitivity of the  $\hat{\mathcal{R}}$  index to  $|p_{\theta\delta}\sqrt{s_{\delta\delta}}|$  (Fig. 4(b)). Other factors seemed to be correlated as well. For example, in the regional simulation, the region size was also correlated to  $|p_{\theta\delta}\sqrt{s_{\delta\delta}}|$  (Fig. 4(b)). Interestingly, TWA measured using the algorithm proposed in [2] was not found as much correlated to  $|p_{\theta\delta}\sqrt{s_{\delta\delta}}|$  as was for the  $\hat{\mathcal{R}}$  index, when considering all regional simulation settings together (Fig. 4(a)). Another interesting result was that both TWA and  $\hat{\mathcal{R}}$  index were sensitive to the spatial dispersion of the repolarization alternans  $s_{\delta\delta}$  (Fig. 2(b) and 2(e)). On the other hand, TWA was sensitive to the global alternans  $\bar{\delta}$  (Fig. 2(a)), whereas almost no correlation was found with  $\hat{\mathcal{R}}$  (Fig. 2(d)). Finally, the third simulations evaluated the error and standard deviation of both  $\hat{\mathcal{R}}$  index and  $\hat{\delta}$  under the effect of noise (Fig. 5). Overall, increasing the SNRs led to a decrease of the errors and standard deviations for both quantities. However, the variance of the  $\hat{\mathcal{R}}$  index was found relatively high even at high SNRs. This result is in line with what previously observed with the  $\mathcal{V}$ -index, in which the standard deviation of its estimator (ratio of two sample variances) was in the order of few milliseconds when computed with 128 beats [35]. Perhaps, an alternative selection of beats and a different algorithm for estimating the lead factors might improve the performance of the sampling scheme and thus obtaining a better effective sample size [36].

The computerized simulations were generated by selecting the values of  $s_{\theta\theta}$ ,  $s_{\delta\delta}$ ,  $p_{\theta\delta}$ ,  $\bar{\delta}$ ,  $\sigma_{\phi}$  and  $\sigma_{\bar{\phi}}$ . To the best of our knowledge, physiological ranges of these quantity for human ventricles are not available. The only two quantities for which a range is plausibly known are  $\sqrt{s_{\theta\theta}}$  and  $\sigma_{\bar{\phi}}$ . The range for the former is supported by the fact that, in all our previous studies concerning the clinical evaluation of the  $\mathcal{V}$ -index, *i.e.*, an estimate of  $\sqrt{s_{\theta\theta}}$ , the values found for healthy subjects were in the range of 20-30 ms [16], [29], [32]. The range for  $\sigma_{\bar{\phi}}$ , as previously described in Section II-C, resembles the QT variability that is known to be  $< 5$  ms in humans. For all other quantities, we relied to electrophysiological studies on animal models. Values of  $\sigma_{\phi}$  below 2 ms were found in rat

myocytes at stimulation rate  $> 1$  Hz [15]. In Guinea pigs, values of  $\bar{\delta}$  were observed up to 70 ms [18] at very high stimulation rates  $> 300$  bpm. We therefore employed a maximum value of 20 ms to account for lower heart rates. The Pearson's correlation coefficient between a measure of repolarization alternans and APD was found approximately 0.7 [6]. Similarly, repolarization alternans was found to vary up to 40% with respect to baseline conditions [6] and this motivated the maximum value of  $\alpha = 0.4$ , leading to a maximum  $\sqrt{s_{\delta\delta}} \approx 13$  ms.

When quantified on the STAFF-III dataset, the  $\hat{\mathcal{R}}$  index was also able to track the time evolution of the inflation, and it compared well with TWA measured on the surface ECG (Fig. 6). Both TWA and  $\hat{\mathcal{R}}$  index were found to increase from the first to the fourth minute of inflation. Interpreting what  $\hat{\mathcal{R}}$  index captured is challenging. However, several possible interpretations can be inferred, based on the fact the correlation  $p_{\theta\delta}$  might exist (as supported by [6]) or not, and might change over time due to prolonged inflations. A plausible time course could be the following. First, the onset of the inflation fired the starting of the repolarization alternans. Second, the prolonged inflation caused a progressive calcium overload [6], [7], resulting in an increase of the correlation  $p_{\theta\delta}$  and spatial variance  $s_{\delta\delta}$  (or only one of them). Third, the release of the inflation reestablished the basal quantity of calcium, bringing back the  $\hat{\mathcal{R}}$  index to pre-inflation levels (Fig. 6(b)).

Speculating about which between  $p_{\theta\delta}$  and  $s_{\delta\delta}$  had played the major role in the observed increase of the  $\hat{\mathcal{R}}$  index during the four minutes of the stimulation is challenging. It is reasonable to believe that the repolarization alternans  $a_m$  is not independent from the electrophysiological properties of the myocyte and its neighborhood. Indeed, characteristics of the myocyte, such as conductances of the ion channels, as well as the local tissue properties, such as electrotonic coupling and fiber directions, limit the capacity of alternating. Plausibly,  $p_{\theta\delta}$  is a quantity describing the whole ventricular tissue at a given HR, and  $s_{\delta\delta}$  is what increased when ischemia was induced. Further investigations are needed to support this statement. Similar reasoning might hold under an ongoing arrhythmia (e.g., tachycardia). Perhaps, data from animal models and exercise stress testing may shed some light on this phenomenon.

The value of  $\sigma_{\bar{\phi}}$  represents the variability of  $\bar{\phi}_k$  or, in other words, the beat-to-beat changes in the average repolarization time  $\bar{\rho}_k$ . This quantity models the fact that during stationary conditions (e.g., stable HR) repolarization times have temporal (beat-wise) variability likely due to the interactions with the autonomic nervous system. Given the fact that  $\bar{\phi}_k$  is a change in the average repolarization time that occurs equally for all myocytes in the  $k$ -th beat, according to the ESS model in (1), its effect is related with a temporal shift of the T-wave. Therefore, the value  $\sigma_{\bar{\phi}}$  characterizes part of the QT variability. Our results are in line with those of Murabayashi et al. [37] that quantified an increased QT variability during ischemic episodes on a different dataset. However, they did not report that QT variability changed over time by returning to baseline values as in our case (Fig. 6(c)). This is probably due to the fact that repolarization alternans, known to appear during ischemia [2], was not considered in the QT variability computation. Indeed, considering all beats together, QT variability becomes sensitive to changes in the

repolarization alternans  $a_m$ , while our  $\sigma_{\bar{\phi}}$  is not by construction. It is worth noting that Murabayashi et al. analyzed ECG segments of 5 minutes, thus making their temporal tracking not fine enough to detect adaptation on the minute-by-minute basis. Another possible explanation for such adaptation could be the direct influence of the HR on  $\sigma_{\bar{\phi}}$ . However, we found an increase of HR only between the pre-operation room and first minute of inflation ( $\Delta\text{HR}$ : median 7.50 IQR (1.30, 13.67) bpm;  $p < 0.05$ ) while it remained stable for the next minutes. Therefore, we can discard that the adaptation was merely due to changes in HR.

Regarding the estimates of  $\bar{\delta}$ , we found that most values were around 0 ms with some exceptions for a small proportion of ECG windows during the fourth minute of inflation. This result suggest that the alternans induced by the occlusions was mostly altering the T-wave morphology rather than shifting it. Linked with our speculation related to  $\sigma_{\bar{\phi}}$  and QT variability, a larger value of  $\hat{\delta}$  in the last minute of the protocol might have contributed to the increase in QT measured by Murabayashi et al. [37] during ischemia. We leave the comparison between  $\sigma_{\bar{\phi}}$ ,  $\bar{\delta}$  and QT variability for future investigations.

The main application scenario for the proposed indexes concerns the risk stratification of SCD. In this study, our intention was to introduce the indexes in such a way that they were solidly grounded on what observed at the cellular level and mathematically sound, and to verify whether they were sensitive to TWA on a dataset in which it was previously observed. Therefore, risk stratification will be the topic of our future investigations. For example, long QT syndrome may be a suitable scenario for the testing of the proposed indexes. Indeed, TWA was already observed in these patients [38] and alternation of calcium concentration seems one of the most important factor [39].

The study has some limitations. First, the model assumed the repolarization alternans to be stationary and the quantities  $\mathcal{R}$ ,  $\bar{\delta}$  and  $\bar{\phi}_k$  were defined upon this assumption. In practice, the stationary condition was mitigated by requiring a stable HR in the analyzed ECG segment. Second, the STAFF-III dataset contained patients that experienced a prior myocardial infarction. However, no difference in terms of TWA was previously reported between the two groups of patients [2]. Third, the model used to validate the  $\mathcal{R}$  index was the same on which the index was based on (i.e., ESS model). However, simulations of synthetic ECGs generated by other biophysically detailed models of human ventricular electrophysiology as mono- and bi-domain models [40], [41] showed that this is not a problem for the  $\mathcal{V}$ -index on which the  $\mathcal{R}$  index is based [42].

## VI. CONCLUSION

In this study, we presented a new model of TWA linking the alternans occurring at the action potential level with the surface ECG. It is shown that surface TWA largely depends on the alternating AP duration and on the spatial covariance between repolarization time and its alternating part. Using the model, we derived the  $\mathcal{R}$  index, computable from the ECG, selectively sensitive to the mentioned spatial covariance, and proposed two algorithms to estimate both  $\mathcal{R}$  and  $\bar{\delta}$ , giving a more complete and detailed description of the alternating phenomena than with the TWA by itself. We tested the metrics on both

computerized simulations and surface ECG where TWA was caused by regional ischemia generated by balloon inflation during PTCA. According to the model, the metrics may reveal new complementary insights in the mechanisms underlying TWA and might be worth exploring it as a new diagnostic/prognostic marker for SCD.

## REFERENCES

- [1] S. Narayan, "T-wave alternans and the susceptibility to ventricular arrhythmias," *J. Amer. College Cardiol.*, vol. 47, no. 2, pp. 269–281, 2006.
- [2] J. P. Martínez, S. Olmos, G. Wagner, and P. Laguna, "Characterization of repolarization alternans during ischemia: Time-course and spatial analysis," *IEEE Trans. Biomed. Eng.*, vol. 53, no. 4, pp. 701–711, Apr. 2006.
- [3] V. Monasterio et al., "Average T-wave alternans activity in ambulatory ECG records predicts sudden cardiac death in patients with chronic heart failure," *Heart Rhythm*, vol. 9, no. 3, pp. 383–389, 2012.
- [4] N. Takasugi et al., "Prevalence of microvolt T-wave alternans in patients with long QT syndrome and its association with Torsade de Pointes," *Circulation: Arrhythmia Electrophysiol.*, vol. 9, no. 2, 2016, Art. no. e003206.
- [5] A. Aro, T. V. Kentt, and H. V. Huikuri, "Microvolt T-wave alternans: Where are we now?," *Arrhythm Electrophysiol. Rev.*, vol. 5, no. 1, pp. 37–40, 2016.
- [6] B.-R. Choi and G. Salama, "Simultaneous maps of optical action potentials and calcium transients in guinea-pig hearts: Mechanisms underlying concordant alternans," *J. Physiol.*, vol. 529, pp. 171–188, 2000.
- [7] F. M. Merchant, O. Sayadi, K. Moazzami, D. Puppala, and A. A. Armondas, "T-wave alternans as an arrhythmic risk stratifier: State of the art," *Curr. Cardiol. Rep.*, vol. 15, no. 9, 2013, Art. no. 398.
- [8] J. M. Pastore, S. D. Girouard, K. R. Laurita, F. G. Akar, and D. S. Rosenbaum, "Mechanism linking T-wave alternans to the genesis of cardiac fibrillation," *Circulation*, vol. 99, no. 10, pp. 1385–1394, 1999.
- [9] J. P. Martínez and S. Olmos, "Methodological principles of T-wave alternans analysis: A unified framework," *IEEE Trans. Biomed. Eng.*, vol. 52, no. 4, pp. 599–613, Apr. 2005.
- [10] J. Coll-Font, B. Erem, and D. H. Brooks, "A potential-based inverse spectral method to noninvasively localize discordant distributions of alternans on the heart from the ECG," *IEEE Trans. Biomed. Eng.*, vol. 65, no. 7, pp. 1554–1563, Jul. 2018.
- [11] A. van Oosterom, "Genesis of the T wave as based on an equivalent surface source model," *J. Electrocardiol.*, vol. 34, pp. 217–227, 2001.
- [12] A. van Oosterom, "The dominant T wave and its significance," *J. Cardiovasc. Electrophysiol.*, vol. 14, pp. S180–S187, 2003.
- [13] P. Laguna, J. P. Martínez, and E. Pueyo, "Techniques for ventricular repolarization instability assessment from the ECG," *Proc. IEEE*, vol. 104, no. 2, pp. 392–415, Feb. 2016.
- [14] M. Zaniboni, A. E. Pollard, L. Yang, and K. W. Spitzer, "Beat-to-beat repolarization variability in ventricular myocytes and its suppression by electrical coupling," *Amer. J. Physiol. Heart Circulatory Physiol.*, vol. 278, no. 3, pp. H677–H687, 2000.
- [15] M. Zaniboni, F. Cacciani, and N. Salvarani, "Temporal variability of repolarization in rat ventricular myocytes paced with time-varying frequencies," *Exp. Physiol.*, vol. 92, no. 5, pp. 859–869, 2007.
- [16] R. Sassi and L. T. Mainardi, "An estimate of the dispersion of repolarization times based on a biophysical model of the ECG," *IEEE Trans. Biomed. Eng.*, vol. 58, no. 12, pp. 3396–3405, Dec. 2011.
- [17] M. W. Rivolta, J. P. Martínez, R. Sassi, and P. Laguna, "Appendix for 'Spatial correlation between myocyte's repolarization times and their alternans drives T-wave alternans on the ECG'," 2022. [Online]. Available: <https://github.com/MassimoWRivolta/iee-jbhi-twa-rpa>
- [18] J. M. Pastore and D. S. Rosenbaum, "Role of structural barriers in the mechanism of alternans-induced reentry," *Circulation Res.*, vol. 87, no. 12, pp. 1157–1163, 2000.
- [19] M. Baumert et al., "QT interval variability in body surface ECG: Measurement, physiological basis, and clinical value: Position statement and consensus guidance endorsed by the European heart rhythm association jointly with the ESC working group on cardiac cellular electrophysiology," *Europace*, vol. 18, no. 6, pp. 925–944, 2016.
- [20] C. D. Woody, "Characterization of an adaptive filter for the analysis of variable latency neuroelectric signals," *Med. Biol. Eng.*, vol. 5, no. 6, pp. 539–553, 1967.
- [21] A. van Oosterom and T. Oostendorp, "ECGSIM: An interactive tool for studying the genesis of QRST waveforms," *Heart*, vol. 90, no. 2, pp. 165–168, 2004.
- [22] F. Palmieri et al., "ECG-based monitoring of blood potassium concentration: Periodic versus principal component as lead transformation for biomarker robustness," *Biomed. Signal Process. Control*, vol. 68, 2021, Art. no. 102719.
- [23] G. B. Moody, W. Muldrow, and R. G. Mark, "A noise stress test for arrhythmia detectors," *Comput. Cardiol.*, vol. 11, pp. 381–384, 1984.
- [24] A. Goldberger et al., "PhysioBank, PhysioToolkit, and PhysioNet: Components of a new research resource for complex physiologic signals," *Circulation*, vol. 101, pp. E215–E220, 2000.
- [25] J. García, P. Lander, L. Sörnmo, S. Olmos, G. Wagner, and P. Laguna, "Comparative study of local and Karhunen-Loève-based ST-T indexes in recordings from human subjects with induced myocardial ischemia," *Comput. Biomed. Res.*, vol. 31, no. 4, pp. 271–292, 1998.
- [26] J. Pettersson et al., "Spatial, individual and temporal variation of the high frequency QRS amplitudes in the 12 standard electrocardiographic leads," *Amer. Heart J.*, vol. 139, pp. 352–358, 2000.
- [27] A. L. Goldberger et al., "PhysioBank, PhysioToolkit, and PhysioNet: Components of a new research resource for complex physiologic signals," *Circulation*, vol. 101, no. 23, pp. E215–E220, Jun. 2000.
- [28] J. P. Martínez, O. Pahlm, M. Ringborn, S. Warren, P. Laguna, and L. Sörnmo, "The STAFF III database: ECGs recorded during acutely induced myocardial ischemia," *Comput. Cardiol.*, vol. 44, pp. 266–133, 2017.
- [29] M. W. Rivolta, L. T. Mainardi, and R. Sassi, "Quantification of ventricular repolarization heterogeneity during moxifloxacin or sotalol administration using V-index," *Physiol. Meas.*, vol. 36, no. 4, pp. 803–811, 2015.
- [30] E. Lepeschkin and B. Surawicz, "The measurement of the Q-T interval of the electrocardiogram," *Circulation*, vol. 6, pp. 378–388, 1952.
- [31] R. Sassi et al., "Spatial repolarization heterogeneity and survival in chagas disease," *Methods Inf. Med.*, vol. 53, no. 4, pp. 1–5, 2014.
- [32] V. Corino, M. W. Rivolta, L. Mainardi, and R. Sassi, "Assessment of spatial heterogeneity of ventricular repolarization after multi-channel blocker drugs in healthy subjects," *Comput. Methods Programs Biomed.*, vol. 189, 2020, Art. no. 105291.
- [33] R. Sassi and L. T. Mainardi, "T-wave alternans: Lessons learned from a biophysical ECG model," *J. Electrocardiol.*, vol. 45, no. 6, pp. 566–570, 2012.
- [34] S. B. Prentner, S. J. Shah, J. J. Goldberger, and A. J. Sauer, "Repolarization heterogeneity: Beyond the QT interval," *J. Amer. Heart Assoc.*, vol. 5, no. 5, 2016, Art. no. e003607.
- [35] M. W. Rivolta, L. T. Mainardi, and R. Sassi, "Theoretical and empirical estimates of V-index variability," in *Proc. Comput. Cardiol. Conf.*, 2018, pp. 1–4.
- [36] L. Martino, V. Elvira, and F. Louzada, "Effective sample size for importance sampling based on discrepancy measures," *Signal Process.*, vol. 2017, pp. 386–401, 2018.
- [37] T. Murabayashi, B. Fetisov, D. Kass, E. Nevo, B. Gramatikov, and R. D. Berger, "Beat-to-beat QT interval variability associated with acute myocardial ischemia," *J. Electrocardiol.*, vol. 35, no. 1, pp. 19–25, 2002.
- [38] W. Zareba, A. J. Moss, S. le Cessie, and W. J. Hall, "T wave alternans in idiopathic long QT syndrome," *J. Amer. College Cardiol.*, vol. 23, no. 7, pp. 1541–1546, 1994.
- [39] W. Shimizu and C. Antzelevitch, "Cellular and ionic basis for T-wave alternans under long-QT conditions," *Circulation*, vol. 99, pp. 1499–507, 1999.
- [40] R. H. Clayton et al., "Models of cardiac tissue electrophysiology: Progress, challenges and open questions," *Prog. Biophys. Mol. Biol.*, vol. 104, no. 1–3, pp. 22–48, 2011.
- [41] S. A. Niederer, J. Lumens, and N. A. Trayanova, "Computational models in cardiology," *Nature Rev. Cardiol.*, vol. 16, no. 2, pp. 100–111, 2019.
- [42] R. Sassi, L. T. Mainardi, P. Laguna, and J. F. Rodriguez, "Validation of the v-index through finite element 2D simulations," in *Proc. IEEE Comput. Cardiol. Conf.*, 2013, pp. 337–340.